Frequency-resolved optical gating with the use of second-harmonic generation

K. W. DeLong and Rick Trebino

Combustion Research Facility, MS-9057, Sandia National Laboratories, Livermore, California 94551-0969

J. Hunter and W. E. White

Lawrence Livermore National Laboratory, Livermore, California 94550

We discuss the use of second-harmonic generation (SHG) as the nonlinearity in the technique of frequency-resolved optical gating (FROG) for measuring the full intensity and phase evolution of an arbitrary ultrashort pulse. FROG that uses a third-order nonlinearity in the polarization-gate geometry has proved extremely successful, and the algorithm required for extraction of the intensity and the phase from the experimental data is quite robust. However, for pulse intensities less than ~1 MW, third-order nonlinearities generate insufficient signal strength, and therefore SHG FROG appears necessary. We discuss the theoretical, algorithmic, and experimental considerations of SHG FROG in detail. SHG FROG has an ambiguity in the direction of time, and its traces are somewhat unintuitive. Also, previously published algorithms are generally ineffective at extracting the intensity and the phase of an arbitrary laser pulse from the SHG FROG trace. We present an improved pulse-retrieval algorithm, based on the method of generalized projections, that is far superior to the previously published algorithms, although it is still not so robust as the polarization-gate algorithm. We discuss experimental sources of error such as pump depletion and group-velocity mismatch. We also present several experimental examples of pulses measured with SHG FROG and show that the derived intensities and phases are in agreement with more conventional diagnostic techniques, and we demonstrate the high-dynamic-range capability of SHG FROG. We conclude that, despite the above drawbacks, SHG FROG should be useful in measuring low-energy pulses.

1. INTRODUCTION

The measurement of the intensity and the phase of an ultrashort laser pulse has been a long-standing unsolved problem. Most available methods, such as second-harmonic generation (SHG) autocorrelation, provide limited intensity information and no phase information.[1,2] Interferometric SHG autocorrelation and induced-grating autocorrelation[3,4] are equivalent to measuring only the spectrum and the intensity autocorrelation of the pulse and thus require *a priori* assumptions about the functional form of the pulse envelope. A few recently developed methods do give the intensity and the phase[5,6] but are experimentally unwieldy and cannot easily be adapted to single-shot operation. Linear measurement techniques cannot give any phase information unless modulators or detection systems with several hundreds of gigahertz of bandwidth are used.[7-9] This is not feasible with currently available technology.

Recently, the technique of frequency-resolved optical gating (FROG) was introduced.[10-12] FROG overcomes all the limitations mentioned above. It can determine the intensity and phase evolution of an arbitrary ultrashort pulse on a single-shot or multishot basis. The experimental apparatus is simple and can be assembled within a day once the components are available. FROG is not interferometric and is often automatically phase matched, so that no critical alignment is needed. FROG has been demonstrated in the ultraviolet, the visible, and the infrared for pulse intensities from 20 kW

to 1 GW (2 nJ to 100 μJ for a 100-fs pulse), where the lower-power figure represents that used for the results presented in the present paper. It has been demonstrated in both single-shot and multishot configurations on pulses that are nearly transform limited as well as in pulses with linear chirp and spectral and temporal cubic phase distortions.[10,12,13] FROG consists of two main parts: first, an experimental apparatus in which two replicas of the pulse to be measured are mixed in a nonlinear-optical medium, and one spectrally resolves the resulting mixing signal as a function of the time delay between the two replicas to create a so-called FROG trace, and second, a phase-retrieval-based algorithm that extracts the complete intensity and phase evolution from the experimentally generated FROG trace.

The FROG technique can use any nearly instantaneously responding nonlinear optical response. Second- and third-order nonlinearities are optimal choices for the technique. Recent research has focused on $\chi^{(3)}$-based nonlinearities for several reasons. First, the FROG traces generated by third-order nonlinearities are more intuitively appealing than second-order traces.[14] For almost all pulses of interest the $\chi^{(3)}$-FROG trace is essentially a plot of the instantaneous frequency as a function of time and is therefore extremely valuable as a real-time monitor of pulse parameters. The FROG trace generated with SHG is not nearly so intuitive and is not so well suited as a real-time pulse monitor. Also, whereas the third-order techniques are complete and unambiguous, second-order techniques contain a time-reversal am-

biguity, which is troublesome. However, when pulse intensities are limited (below approximately 1 MW), a second-order technique would appear necessary because of its enhanced signal strength compared with third-order techniques.

FROG with the use of SHG was first proposed and discussed, and the temporal ambiguity identified, in the initial FROG publications and patent.[11,12,15] It was noted in these references that SHG FROG would be useful for low-power pulses. The first experimental realization of SHG FROG was recently published,[16] along with a slightly modified version of the original FROG pulse-retrieval algorithm used for polarization-gate (PG) FROG. Unfortunately, this modified algorithm converges for only a limited set of pulses and thus is unsatisfactory. As a result, we have developed a new, improved algorithm that uses the concept of generalized projections, a more elegant, well-established technique that enables the algorithm to converge for an extremely large set of pulses. However, even with this improvement, and availing ourselves of the additional techniques developed to aid the PG FROG algorithm,[17] there are still pulses (such as shaped pulses with complicated intensity substructure) for which this improved SHG FROG algorithm has difficulty. For this reason, among others, it should be noted that, at present, $\chi^{(3)}$-based FROG techniques are to be preferred whenever sufficient pulse power is available.

Nevertheless, there are many cases in which insufficient pulse power dictates the use of SHG FROG. Consequently, in this paper we present a thorough exploration of the theoretical, algorithmic, and experimental issues peculiar to SHG FROG. We review the theoretical framework of SHG FROG and discuss the temporal ambiguity and its consequences. We review the basic FROG algorithm and present the new algorithm. We discuss experimental issues peculiar to SHG FROG that arise from the nature of the second-order nonlinear process. We then present the results of experimentally measured pulses, including a verification of SHG FROG by comparison with other pulse diagnostics, namely, the autocorrelation and the spectrum. We also demonstrate the use of SHG FROG in measuring a higher-order phase distortion and confirm the measurement of a pulse with a known amount of linear chirp. Finally, we discuss an advantage of SHG FROG: its ability to make high-dynamic-range measurements.

2. THEORY

The FROG technique involves splitting the pulse to be measured into two replicas and crossing them in a nonlinear-optical medium (see Fig. 1). The nonlinear mixing signal is then spectrally resolved as a function of the time delay between two beams. In the case of SHG FROG the noncollinear autocorrelation signal generated in a frequency-doubling crystal is the nonlinear signal. The envelope of the SHG FROG signal field therefore has the form

$$E_{\text{sig}}(t, \tau) = E(t)E(t - \tau), \qquad (1)$$

where $E(t)$ is the complex envelope of the pulse to be measured (the carrier frequency has been removed) and τ

is the delay between the two beams. This signal is then used as the input to a spectrometer, and the intensity is detected by a photodiode or CCD array to yield the FROG trace

$$I_{\text{FROG}}(\omega, \tau) = \left| \int_{-\infty}^{\infty} dt\, E_{\text{sig}}(t, \tau) \exp(i\omega t) \right|^2$$

$$= |E_{\text{sig}}(\omega, \tau)|^2. \qquad (2)$$

The FROG trace is a positive real-valued function of two variables: the frequency and the time delay between the two pulses. This experimentally determined FROG trace is then used as an input to a numerical algorithm, which determines the full complex electric field, i.e., both the intensity and the phase, of the pulse that created the FROG trace.

Note that the signal field of Eq. (1) is invariant (except for a trivial temporal offset) with respect to a change of sign of the delay time τ, so that the SHG FROG trace is always symmetric about τ: $I_{\text{FROG}}(\omega, \tau) = I_{\text{FROG}}(\omega, -\tau)$. This leads to an ambiguity in the retrieved electric field with respect to time, such that the field $E(t)$ yields the same FROG trace as $E^*(-t)$ (the complex conjugate here appears because we restrict ourselves to the positive frequency components of the field). This temporal ambiguity is the main shortcoming of SHG FROG compared with the $\chi^{(3)}$ FROG method. Not only is ambiguity in the retrieved field undesirable in itself but it also leads to unintuitive traces and creates problems in the pulse-retrieval algorithm, as we will see in Section 3 below.

To illustrate these points, consider a pulse with a Gaussian intensity profile and a linear chirp, written as[18]

$$E(t) = \exp(-at^2 + ibt^2). \qquad (3)$$

The normalized SHG FROG trace of this field can be shown to be

$$I_{\text{FROG}}(\omega, \tau) = \exp\left[\frac{-4(a^3 + ab^2)\tau^2 - a\omega^2}{4(a^2 + b^2)} \right]. \qquad (4)$$

The SHG FROG trace of a linearly chirped pulse is an untilted ellipse that is independent of the sign of the chirp parameter b. In other words, the SHG FROG trace is identical for a pulse with positive or negative linear chirp. This is to be contrasted with PG FROG traces, where pulses with positive or negative linear chirp yield ellipses tilted to have a positive or negative slope, respectively, so that positive and negative chirp are easily distinguished. In general, SHG FROG cannot distinguish between a pulse and its time-reversed replica. One must employ
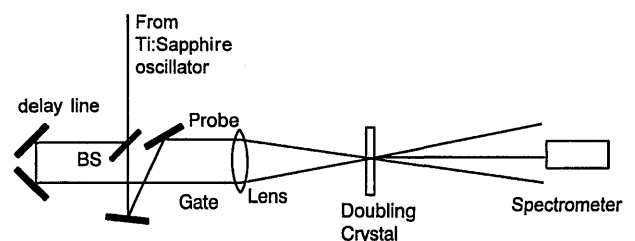
Fig. 1. SHG FROG experimental setup. BS, Beam splitter.

some other, as yet undetermined, method to ascertain the direction of time for pulses retrieved with SHG FROG.

Note that the temporal ambiguity affects only phase distortions that are even functions of time. Linear chirp, which has a quadratic temporal phase dependence, has an ambiguous sign in SHG FROG. However, a frequency shift (a linear phase in time) or a temporal cubic phase distortion (a cubic phase in time) does not have an ambiguous sign. All orders of phase distortions specified in the frequency domain appear to have ambiguous signs in SHG FROG, however.

Practically speaking, this ambiguity is not so restrictive as it might appear. We often have some *a priori* knowledge of the pulse that we can use in removing this ambiguity. For example, pulses generally acquire positive linear chirp (unless one is working in the negative group-velocity-dispersion regime) as a result of propagation through normal optics. Therefore one can determine the direction of time of the retrieved pulse by requiring the pulse to have a positive, rather than a negative, linear chirp component. Also, for high-intensity pulses, some self-phase modulation may occur. When the sign of the nonlinear refractive index n_2 is known, as it is for most materials, we can again ascertain the direction of time by specifying the proper sign of the phase.

Another way in which one can remove the temporal ambiguity is to obtain a second FROG trace of the pulse after adding some known phase distortion to the pulse. For example, one could generate a second FROG trace after passing the pulse through a known thickness of glass. By directly subtracting the phases of the two retrieved pulses and knowing the group-velocity dispersion of the glass, one can easily determine whether the original pulse was positively or negatively chirped (an originally positively chirped pulse will move farther from the transform limit when passing through a material with positive group-velocity dispersion, and vice versa).

It should be noted that, although the SHG FROG trace is symmetric with respect to τ, this restriction does not apply to the pulse derived with the algorithm. If we use a temporally asymmetric pulse to generate a SHG FROG trace, the pulse-retrieval algorithm will output that asymmetric pulse (or its time-reversed replica). We will see an example of such a pulse below.

3. ALGORITHM

Once we have experimentally generated the FROG trace in the laboratory, we must apply a numerical algorithm to the data in order to determine the complete complex envelope.[12,17] This algorithm is based on the iterative Fourier-transform algorithms used in phase-retrieval problems.[19] The family of FROG algorithms is actually more robust than standard phase-retrieval algorithms, partially because of the existence of the constraint specified by Eq. (1), which is not available in, for example, image-recovery problems.

The original basic FROG algorithm (developed for PG FROG) published previously[10,12] is not so effective at SHG FROG as it is for PG FROG. A slightly modified version of this algorithm,[10] which included the application of a spectral constraint, has also been suggested specifically for SHG FROG (henceforth we call that algorithm

the modified basic algorithm). Unfortunately, neither of these algorithms converges for the types of pulse commonly observed, so we have found it necessary to introduce a more mathematically powerful and elegant (as well as intuitive) algorithmic technique, known as generalized projections.[20] Here we compare the performance of these three algorithms.

We tested all three algorithms on a series of pulses (namely, pulses with linear chirp, self-phase modulation, temporal and spectral cubic phase distortion, and coherent sums of as many as four Gaussian pulses with varying amounts of self-phase modulation) in the absence of noise. This set of pulses is the same set that we used previously to test the PG FROG algorithm.[17] We applied the same criterion for convergence as that in Ref. 17, namely, the root-mean-square (rms) error between the original FROG trace and the trace generated by the retrieved field. This is constructed as

$$G = \left\{ \frac{1}{N^2} \sum_{\omega,\tau=1}^{N} [I_{\mathrm{FROG}}(\omega,\tau) - |E_{\mathrm{sig}}(\omega,\tau)|^2]^2 \right\}^{1/2}. \quad (5)$$

Both I_{FROG} and $|E_{\mathrm{sig}}|^2$ are normalized to a peak value of unity before G is computed. A value of G less than 0.0001 is defined as convergence for noise-free (numerically simulated) pulses. At this level of error the retrieved field is visually indistinguishable from the original field.

The three algorithms that we tested are the basic algorithm,[12] the modified basic algorithm,[16] and the complete, composite algorithm, which uses generalized projections (developed in this paper and described in Section 4 below) as well as a host of other techniques developed for PG FROG.[17] These results are summarized in Table 1.

We have found that the SHG FROG algorithms are more sensitive to the initial guess than is the PG FROG algorithm (which is relatively insensitive to the initial guess). As a result, we have considered two different initial guesses for each algorithm. The first is a pulse with a Gaussian intensity profile and random phase noise, labeled Noise in Table 1. The other initial guess, labeled Smooth, is a Gaussian pulse with a slight linear chirp (1% over the transform limit) plus a small (1% in intensity) satellite pulse, located 1.1 FWHM away from the main pulse. The asymmetric smooth initial guess appears to improve convergence for asymmetric pulses.

Table 1 demonstrates the superiority of the full algorithm. The other algorithms are satisfactory for only the simplest possible pulses, whereas the full algorithm converges for practically every pulse. Using the full algorithm, we were able to retrieve all but one of the test pulses with the smooth initial guess, and that pulse was easily retrieved with the random-phase-noise initial guess. The full algorithm was also much more successful at retrieving experimental pulses, or pulses with noise added to the FROG trace. Most of the noise-free pulses converged within 100–200 iterations, where each iteration required roughly 1 s on a 20-MHz, R2000-based UNIX workstation.

The modified basic algorithm presented earlier[16] employs a spectral constraint in order to aid convergence. Spectral constraints were found to be ineffective in PG FROG.[17] On the other hand, we have found that a

Table 1. Comparison of the Various SHG FROG Algorithms[a]

Initial Guess	Basic Algorithm		Modified Algorithm		Full Algorithm with Projections	
	Noise	Smooth	Noise	Smooth	Noise	Smooth
Trans. Lim.	Yes	Yes	Yes	Yes	Yes	Yes
Lin. Chirp	Yes	Yes	Yes	Yes	Yes	Yes
SPM	Yes	Yes	No	No	Yes	Yes
SPM + P.L.	No	No	No	No	Yes	Yes
SPM + N.L.	No	No	Yes*	Yes*	Yes	Yes
TCP	Yes	Yes	No	No	Yes	Yes
SCP	Yes	Yes*	No	Yes*	Yes	Yes
Double	Yes	Yes	No	No	Yes	Yes
Satellite	No	Yes*	No	Yes	No	Yes
Complex	12%	12%	25%	0%	81%	94%
Total	36%		36%		100%	

[a]The simulated SHG FROG trace data were calculated on a 64×64 grid, and we employed Gaussian pulses with a FWHM of $\tau_{FW} = 10$ units unless otherwise stated. Functional forms of the electric fields are the same as those in Ref. 14. The types of pulse are as follows. Trans. Lim.: transform-limited; Lin. Chirp: linearly chirped, with chirp parameter $b = 4/\tau_{FW}{}^2$, where the phase $\phi(t) = bt^2$; SPM: self-phase modulated, with $Q = 3$ rad of phase change at the peak of the pulse; SPM + P.L.: a self-phase-modulated pulse combined with positive linear chirp (same magnitudes as those above); SPM + N.L.: a self-phase-modulated pulse combined with negative linear chirp; TCP: temporal cubic phase, with chirp parameter $c = 4/\tau_{FW}{}^3$, where the phase $\phi(t) = ct^3$; SCP: spectral cubic phase, with a FWHM of 5 and chirp parameter $d = \tau_{FW}{}^3/6.25$, where the phase $\phi(\omega) = d\omega^3$; double: a double-peaked pulse (FWHM = 6), with $B = 1$ (equal intensities) and separation $D = 12$; satellite: a double pulse (FWHM = 6), with $B = 0.3$ (9% intensity) and $D = 12$; complex: a set of 16 different pulses, each a coherent sum of four Gaussian pulses with various widths, heights, and positions, both with and without SPM (the percentage indicated here shows what percentage of these pulses were retrieved). The columns headed Noise used a pulse with a Gaussian intensity profile and random phase noise as an initial guess, and the column heading Smooth indicates a Gaussian pulse with linear chirp (1% above the transform limit) and a satellite pulse with an intensity 1% that of the main pulse, located 1.1 FWHM from the main pulse. An asterisk indicates that the retrieved field was visually quite close to the correct field but the criterion for convergence defined in Ref. 17 was not met. Total refers to the percentage of pulses retrieved for all initial guesses and all 25 pulse types used.

spectral constraint is helpful in SHG FROG, but only if the spectrum is accurate and noise free. We have found that constraining the field to match an inaccurate spectrum is quite effective at preventing convergence. The method used to generate the pulse spectrum from the FROG trace in Ref. 16, involving multiple Fourier transforms and square-root operations, is susceptible to noise and aliasing effects and often yields a somewhat inaccurate spectrum, even in the absence of noise. It is possible that well-known, more reliable, iterative deconvolution methods might better extract the spectrum from the SHG FROG trace, but we believe that the use of a spectral constraint should be avoided when possible. The improved full algorithm discussed here does not employ the use of a spectral constraint.

A source of difficulty for the basic FROG algorithm in SHG FROG appears to be the existence of the temporal ambiguity. One failure mode for the basic algorithm is stagnation at a pulse shape that appears to be a combination of the correct pulse and its time-reversed replica, which has the same FROG trace. (For example, in attempting to retrieve a linearly chirped pulse, the algorithm may stagnate on a pulse that has positive linear chirp over part of its extent and negative linear chirp over the rest of the pulse.) We believe that this pathology is a manifestation of the temporal ambiguity discussed above. It is also likely that the complex nature of the gate pulse hampers the performance of the SHG FROG algorithm (in PG FROG the gate is a strictly real function).[14]

Another unusual feature of the SHG FROG algorithms is that it appears to be more difficult to retrieve a pulse with a flat phase than a pulse with significant phase distortion. Indeed, when converging to a transform-limited pulse, the algorithm first finds a chirped pulse of equal pulse width and then reduces the chirp until it becomes negligible.

4. GENERALIZED PROJECTIONS

Central to the operation of the improved algorithm mentioned in Section 3 is mathematical concept known as generalized projections.[20] Projections offer a simple way to visualize the operation of these types of iterative algorithm, and they lend themselves to a powerful and straightforward algorithmic implementation that considerably increases the power of the FROG algorithm. We shall now explain the concept of generalized projections.

In the FROG algorithm we are trying to select a signal field $E_{sig}(t, \tau)$ that satisfies two constraints. First, its FROG trace as computed by Eq. (2) must match that of the experimental data (this is constraint 1). Second, it must be a field that can be generated by a physically realizable electric field through Eq. (1) (this is constraint 2). We can imagine a function space of complex two-dimensional functions in which each point represents a single possible $E_{sig}(t, \tau)$. Then the values of $E_{sig}(t, \tau)$ that satisfy the above constraints form two sets, one for each constraint. The intersection of these two sets represents the correct solution, as seen in Fig. 2. Once this correct value of $E_{sig}(t, \tau)$ is found, the proper form of $E(t)$ is easily determined.[10,12]

The method of solution is also seen in Fig. 2. Beginning with an arbitrary starting point, we move to the closest point in the first set. This act of moving to the closest point in a set is called a projection. After projecting the starting point onto set 1, we then project it onto set 2, etc. It is clear from Fig. 2 that, as we alternately project onto the two sets, the trial solution will move closer and closer to the correct solution. This is what is known as the method of projections.
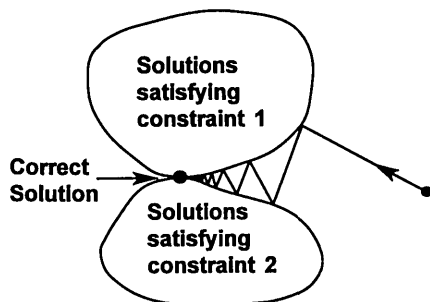
Fig. 2. Illustration of the method of projections. In a space consisting of all possible signal fields the fields that satisfy the constraints of Eqs. (1) and (2) form closed sets. The correct solution to the FROG problem is the intersection of these two sets. In the method of projections we close in on the correct solution as we iteratively move from the surface of one set to that of the other.

The topological shapes of the sets are important in this method. The sets shown in Fig. 2 are convex. This means that a line connecting any two points in the set does not leave the set. It can be shown that for two convex sets the method of projections guarantees convergence. If one or both of the sets are nonconvex, however, there is no mathematical proof of convergence of this method (although in practice it is often the case that the method does converge). In this case (in which one or more of the sets is nonconvex) we speak of the method of generalized projections.

In FROG neither of the constraint sets is convex: the act of constraining the magnitude of the Fourier transform to a prescribed form is a projection onto a nonconvex set,[20] and the set of signal fields that satisfy Eq. (1) is nonconvex because of the nonlinear nature of the signal field. Therefore there is no mathematical guarantee of convergence for any FROG pulse-retrieval algorithm. However, as we have seen in Section 3 above, the application of the method of generalized projections is quite effective in SHG FROG. We will now detail the application of this method to the FROG problem.

The FROG algorithm is diagrammed in Fig. 3. The algorithm begins with a trial solution for the field $E(t)$. We then generate a signal field from that trial field, using Eq. (1), and Fourier-transform it into the (ω, τ) domain. The squared magnitude of this frequency-domain signal field $E_{sig}(\omega, \tau)$ is the FROG trace of the trial field $E(t)$. Now we must apply the first projection, that is, constrain the magnitude of this frequency-domain signal field to the magnitude of the experimentally measured FROG trace. This is accomplished simply by replacement of the magnitude of the frequency-domain signal field with the magnitude (square root) of the experimental FROG trace while the phase is left unchanged:

$$E_{sig}'(\omega, \tau) = \frac{E_{sig}(\omega, \tau)}{|E_{sig}(\omega, \tau)|} [I_{FROG}(\omega, \tau)]^{1/2}. \tag{6}$$

This forms the projection onto the set of signal fields that satisfy constraint 1, as given by Eq. (2).

After the first projection we inverse-Fourier-transform the signal field back into the (t, τ) domain to obtain $E_{sig}'(t, \tau)$. In order to implement the second projection, we must find the signal field that satisfies constraint 2

[Eq. (1)] and that is closest, in some sense, to $E_{sig}'(t, \tau)$. The metric that we use to measure this closeness is given by

$$Z = \sum_{t,\tau=1}^{N} |E_{sig}'(t, \tau) - E(t)E(t - \tau)|^2. \tag{7}$$

The right-hand term inside the squared modulus, $E(t)E(t - \tau)$, forms a new signal field that is guaranteed to be inside constraint set 2. To find the new signal field that is closest to $E_{sig}'(t, \tau)$, we minimize Z with respect to $E(t)$. The new signal field found by this minimization is the field that corresponds to the projection of $E_{sig}'(t, \tau)$ onto the set of fields satisfying Eq. (1), which is constraint set 2. This projection provides us with the guess for $E(t)$ for the next cycle of the algorithm. In practice, we find that it is not necessary to perform a global minimization of the error Z. A single one-dimensional minimization along the direction of the analytically computed gradient of Z seems to suffice and is computationally much faster. This minimization procedure is detailed elsewhere.[17,21] It involves treating the error Z as a single-valued function of $2N$ variables, these being the values of the real and imaginary parts of $E(t)$ at each of the N sampling points of the array that holds the field.

The FROG algorithm as diagrammed in Fig. 3 is structurally the same for the basic FROG algorithm and the algorithm based on generalized projections. The difference between the two is the method in which a new $E(t)$ is generated from $E_{sig}'(t, \tau)$. Previously published algorithms,[12,17] including the basic and modified basic algorithms mentioned in Section 3 above, implemented this second constraint in an *ad hoc* fashion. The use of a projection, as in Eq. (7), in implementing constraint 2 is the main difference between the robust, improved algorithm and the other, less effective algorithms.

The method of generalized projections is then combined with the basic FROG algorithm, as well as other types of FROG retrieval algorithm that we have named overcorrection, intensity constraint, and minimization, as described in an earlier paper.[17] (Note that the intensity-constraint method, which in PG FROG yields the intensity envelope of the pulse, yields a time-reversed version of the field in SHG FROG.) This new composite algorithm monitors its own progress for stagnation and applies new methods when necessary to ensure the maximum possible level of convergence. The combination of the method of generalized projections and the other techniques of the composite algorithm is extremely powerful.
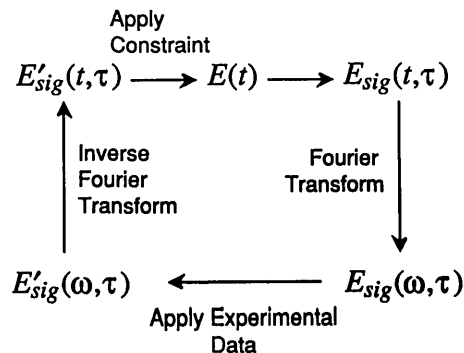
Fig. 3. Schematic of the FROG pulse-retrieval algorithm.

5. EXPERIMENTAL CONSIDERATIONS

There are several issues relevant to performing an SHG FROG experiment and to using the pulse-retrieval algorithm to reconstruct the pulse that created the experimental FROG trace. In this section we will explore some of these issues, such as maximum allowable conversion efficiency and crystal length, finding the zero time delay position, and errors in the data calibration.

The accuracy of the SHG FROG technique depends on maintaining the relationship between the input field and the signal field as written in Eq. (1). This limits the conversion efficiency that one can use when generating the signal field. If the intensity at the crystal, and therefore the SHG efficiency, is too high, depletion of the input fields will occur, and Eq. (1) will no longer be valid.

In order to determine the maximum allowable conversion efficiency in SHG FROG, we consider the full solution for SHG in the presence of pump depletion, given by[22]

$$E_{\mathrm{SHG}}(t) \propto E(t)\tanh[\alpha E(t)], \tag{8}$$

where α is some constant proportional to the length of the crystal and the effective nonlinear coefficient. For low field strengths the SHG field is essentially linear in the square of the input field; however, at high fields, the conversion efficiency decreases as the hyperbolic tangent function departs from a linear behavior. When the argument of the hyperbolic tangent equals 0.174, there is a 1% deviation from linear behavior. This is equivalent to a 3% peak intensity conversion efficiency, which, for Gaussian pulses, translates to a 2.1% energy conversion efficiency. Thus, if we wish to maintain Eq. (1) to within 1%, we must keep the peak intensity conversion efficiency below 3%. This is not a very restrictive constraint.

Another effect that can reduce the accuracy of SHG FROG is group-velocity mismatch in the doubling crystal between the fundamental and second-harmonic beams.[23] Group-velocity mismatch acts as a finite temporal impulse-response function that is convolved with the second-harmonic signal. The width of this response function is

$$t_w = \left(\frac{1}{v_g{}^{\mathrm{SHG}}} - \frac{1}{v_g{}^{\mathrm{fund}}} \right) L, \tag{9}$$

where v_g is the group velocity. In the frequency domain this effect acts as a frequency-dependent filter of the form

$$F(\omega) = \left[\frac{\sin(t_w \omega/2)}{t_w \omega/2} \right]^2 \tag{10}$$

that multiplies the emerging SHG signal spectrum. While this effect was found not to be critical in normal autocorrelation measurements (where one measures only the integrated output SHG signal energy), in SHG FROG it can be quite important (where the spectrum of the SHG signal is needed). The result of this effect is that the pulse retrieved by the SHG FROG algorithm will have a narrower bandwidth than the actual pulse (thus appearing closer to the transform limit than it actually is), and its phase evolution can be highly distorted. It is therefore advisable to keep t_w as small as possible (by the use of thin doubling crystals, for example).

For a fixed pulse length and a given value of t_w the effect of group-velocity mismatch will be least critical for transform-limited pulses, where the bandwidth is narrow, but will affect highly phase-distorted pulses more strongly. For example, for a transform-limited pulse we have found that even a value of t_w equal to the FWHM of the pulse lengthened the retrieved pulse (and narrowed the retrieved spectrum) by only 10%. However, for a self-phase-modulated pulse with 3 rad of peak phase change, a t_w of one half of the pulse FWHM resulted in a retrieved field that was longer by 30% and spectrally narrower by 63% than the actual pulse. In general, we have found that, as long as the half-width at half-maximum of the spectral filter in Eq. (10) (which evaluates to $2.78/t_w$) is larger than 1.4 times the spectral half-width at half-maximum of the SHG signal [which is $4(\ln 2)\sqrt{2}/t_p$ for a transform-limited pulse, according to Eq. (4)], the effects of group-velocity mismatch should introduce a less than 10% error in the retrieved pulse parameters. For a fundamental wavelength of 800 nm and a crystal thickness of 300 μm, t_w is 23.0 fs in potassium dihydrogen phosphate and 56.6 fs in barium borate.

Another issue in data reduction is the symmetrization of the SHG FROG trace. Because the SHG FROG trace is symmetric in time, it is tempting to symmetrize explicitly the experimental SHG FROG traces about the delay axis before we use them in the pulse-retrieval algorithm. While this does indeed reduce the final error between the experimental and reconstructed FROG traces, we have found that this procedure tends to distort the pulses somewhat, for two reasons. First, if the trace has not been centered in delay properly, symmetrizing the trace will broaden it somewhat. Second, symmetrizing the noise on the trace can actually increase its effect. The reason is that the algorithm tends to ignore or smooth over components of the SHG FROG trace that are antisymmetric in delay, since these cannot be generated through Eqs. (1) and (2). Therefore we feel it is best not to symmetrize experimental FROG traces.

When one uses the pulse-retrieval algorithm, it is important to specify the exact location of the $\tau = 0$ point τ_0 in the experimental FROG trace. However, one does not usually know exactly where the zero-time-delay point occurs in the experimental trace. In this case we take advantage of the fact that the zero-order delay margin,

$$M_\tau(\tau) = \int_{-\infty}^{\infty} \mathrm{d}\omega \, I_{\mathrm{FROG}}(\omega, \tau), \tag{11}$$

which is, in fact, the usual second-order intensity autocorrelation in SHG FROG,[14] has its peak at $\tau = 0$. In general, the peak of the zero-order delay margin will not occur at one of the input time delays; that is, the τ_0 point will occur between pixels on the FROG trace. Since the intensity autocorrelation is necessarily symmetric, we have found that the best way to determine the zero-delay position is through a first-moment approach such as

$$\tau_0 = \frac{\int_{-\infty}^{\infty} \mathrm{d}\tau \, \tau M_\tau(\tau)}{\int_{-\infty}^{\infty} \mathrm{d}\tau \, M_\tau(\tau)}. \tag{12}$$

The FROG trace is then shifted to be centered at this value of delay by linear interpolation between adjacent
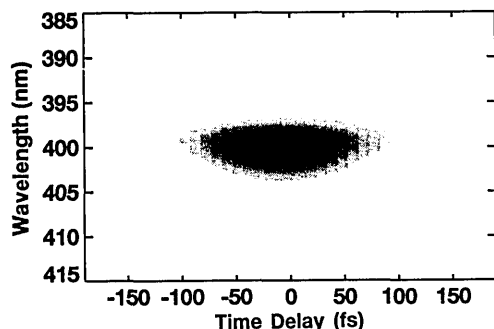
Fig. 4. SHG FROG trace of a laser pulse from a Ti:sapphire oscillator. This trace consists of 39 individual spectra of the autocorrelation of the pulse, each taken at a different time delay.

pixels in the input data. This procedure helps us to achieve a low error between the experimental FROG trace and the reconstructed FROG trace and higher fidelity in the reconstructed pulse. We have found, however, that errors incurred in centering the FROG trace to only the nearest pixel, without interpolating to fractional pixel spacings, are usually quite small.

When putting experimental data into the FROG algorithm, one must specify the size of the increment both in time and in wavelength, as well as the central wavelength of the data. Errors in specifying these parameters will lead to error in the resulting pulses retrieved by the FROG algorithm. We have explored this source of error by taking FROG traces generated by noise-free (numerically simulated) pulses as input data and supplying the algorithm with deliberately incorrect wavelength and time calibrations.

We find that, when these calibrations are inaccurate, the pulse parameters, such as FWHM, spectral width, and amount of phase distortion, are all affected. Generally, the amount of error in these parameters will be of the order of the inaccuracy in the input calibration. For example, if the temporal calibration for the experimental FROG trace is incorrect by 10%, we can expect the parameters of the retrieved pulse to be inaccurate by approximately 10%, to within a factor of 2. The exact amount of error will vary according to the individual pulse. The step sizes in the temporal and frequency domains are related by the Fourier transform, so that errors in the temporal calibration can lead to errors in the spectral width and the amount of phase distortion as well as in the FWHM of the pulse. Errors in specifying central wavelength, which relates the time and wavelength scales, also introduces calibration errors. Also, the functional form of the retrieved pulse will be affected by calibration errors.

These points are illustrated by the following examples, in which calibration factors that were too small were used to retrieve pulses. For a linearly chirped pulse a 20% error in temporal calibration leads to a retrieved pulse that is linearly chirped but with a 20% error in pulse width and is 21% closer to the transform limit. A 20% error in the wavelength calibration leads to a 20% error in the spectral width of the retrieved pulse, which is also 21% closer to the transform limit. For a pulse with self-phase modulation the situation is more complex. A 20% error in specifying the temporal calibration leads to a retrieved pulse with a 33% error in pulse width, a 32% error in spectral

width, and a 28% error in total phase excursion. This retrieved pulse is 36% closer to the transform limit than the initial pulse. A 20% error in specifying the wavelength calibration leads to a 16% error in the retrieved pulse width as well as a 46% error in the spectral width and a 27% reduction in total phase excursion, resulting in a retrieved pulse that is 37% closer to the transform limit than the original pulse. From these results we can see that the effect of incorrect calibrations will be quite different for differing pulses.

6. EXPERIMENTAL RESULTS

We have used SHG FROG to measure pulses from a Spectra-Physics Tsunami Ti:sapphire oscillator operating at a center wavelength of 800 nm. The laser pulse was split into two, and the gate pulse was passed through a variable time delay (realized by a stepper-motor-controlled stage), as in Fig. 1. The two beams were focused at an angle of 0.8° in a background-free autocorrelation geometry into a potassium dihydrogen phosphate crystal (300 μm thick) by a 50-cm focusing lens. The pulse energy at the crystal was 1–2 nJ. The conversion efficiency to the second harmonic was less than 10^{-4}, well within the range dictated by relation (8). The spectrum of the second harmonic was recorded for 39 separate time delays. The spacing between time delays was 10 fs. A background spectrum of dark current and scattered light, taken when the two pulses were delayed by more than 1 ps, was subtracted from all the data. The group-velocity mismatch parameter of the potassium dihydrogen phosphate crystal can be calculated from Eq. (9) to be $t_w = 23$ fs. This value of t_w should not affect the measurements of the transform-limited pulses below; however, for spectrally broader pulses this could become a problem.

FROG traces were obtained for a wide range of operating conditions, and intensity and phase evolutions were obtained with the use of the new algorithm. A typical SHG FROG trace is shown in Fig. 4. The SHG FROG trace appears fairly smooth, with a small asymmetry in the wavelength direction. The SHG FROG trace is symmetric with respect to τ, in agreement with Eq. (1). Using these data as input to the pulse-retrieval algorithm,
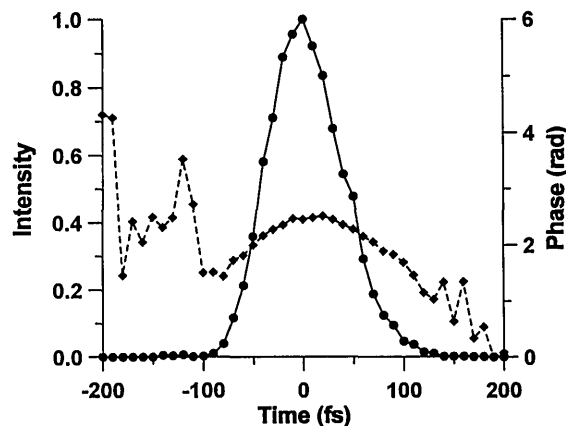
Fig. 5. Intensity (solid curve with circles) and phase (dashed curve with diamonds) of the pulse retrieved from the FROG trace of Fig. 3. The pulse has a 90-fs FWHM. The final FROG error for this retrieved pulse was $G = 0.00156$.
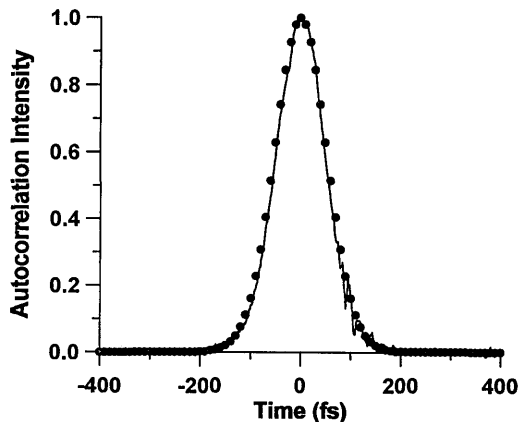
Fig. 6. Measured autocorrelation (solid curve) of the same laser that created the FROG trace of Fig. 3 and numerical autocorrelation (circles) of the retrieved pulse of Fig. 4. The agreement between the laboratory measurement and the pulse retrieved through FROG is excellent.
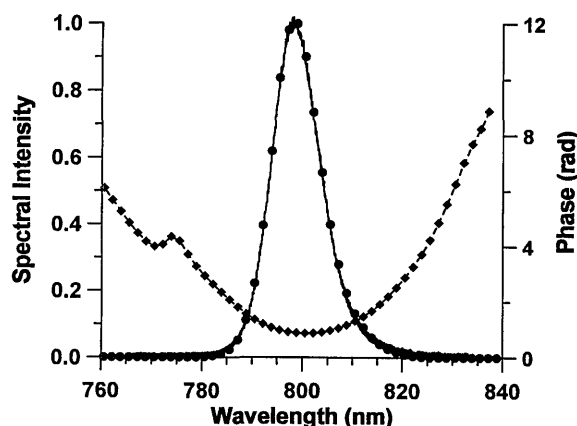
Fig. 7. Comparison of the experimentally measured spectrum (solid curve) of the laser that created the FROG trace of Fig. 3 with the numerically generated spectrum (circles) of the retrieved pulse of Fig. 4. The agreement between the laboratory measurement and the pulse retrieved through FROG is excellent. The phase of the spectrum (dashed curve with diamonds) as retrieved from the FROG pulse-retrieval algorithm is also shown.

we extract the electric field shown in Fig. 5, using a 128×128 pixel FROG trace. The convergence parameter G was 0.00156, a small value for experimental data. We find that this pulse has an intensity FWHM of 90 fs. The pulse has a small amount of phase distortion that is mostly quadratic (linear chirp) with a chirp parameter of $b = 1.3 \times 10^{-4}$ fs^{-2}. The large phase fluctuations seen in the wings of the pulse are inconsequential, as the intensity is extremely low. The time–bandwidth products of this pulse are $\Delta t \Delta f = 0.487$ if we use the (temporal and spectral) FWHM of the pulse and $\Delta t \Delta \omega = 0.708$ if we use the rms measure of pulse (temporal and spectral) width. The time–bandwidth products for a transform-limited Gaussian pulse are 0.441 and 0.5, respectively. We find that the pulse rms (FWHM) intensity width is broadened by 17% (60%) over the transform-limited pulse (defined as the inverse Fourier transform of the pulse spectrum with a flat phase). Similarly, the rms (FWHM) spectral broadening caused by the nonzero temporal phase of the pulse is 23% (12%). It is difficult to

understand the amount of phase distortion from such measures, illustrating once again the importance of measuring the intensity and the phase of the pulse directly with a technique such as FROG.

In order to ascertain the accuracy of the retrieved pulse, we can make a comparison with the independently measured autocorrelation and spectrum of the pulse, two easily measured and well-understood quantities. We measured the autocorrelation of this pulse, using a Femtochrome autocorrelator, and we also measured the spectrum of the pulse with a spectrometer. We now compare these experimental quantities with the analogous ones calculated numerically with the pulse depicted in Fig. 5. The comparison is shown in Figs. 6 and 7. Figure 6 shows the experimentally measured autocorrelation of the pulse as well as the numerical autocorrelation of the pulse retrieved by the algorithm. The agreement is remarkable, and the two curves are practically indistinguishable. Figure 7 shows a similar comparison for the spectrum. Again, the agreement is excellent. The pulse retrieved by SHG FROG is thus in excellent agreement with the autocorrelation and the spectrum of the laser pulse.

The method of SHG FROG is also able to retrieve pulses with more complicated phase profiles. Figure 8 shows the SHG FROG trace of a pulse from the Ti:sapphire
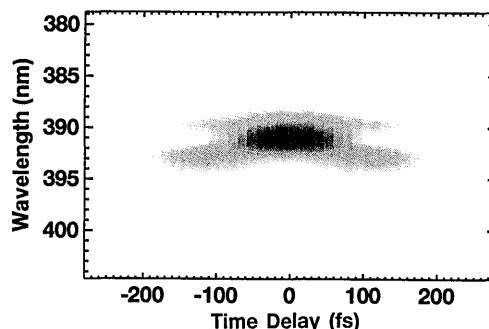
Fig. 8. SHG FROG trace of a pulse from a Ti:sapphire oscillator with excess glass in the cavity. The horseshoe characteristic is indicative of spectral cubic phase distortion.
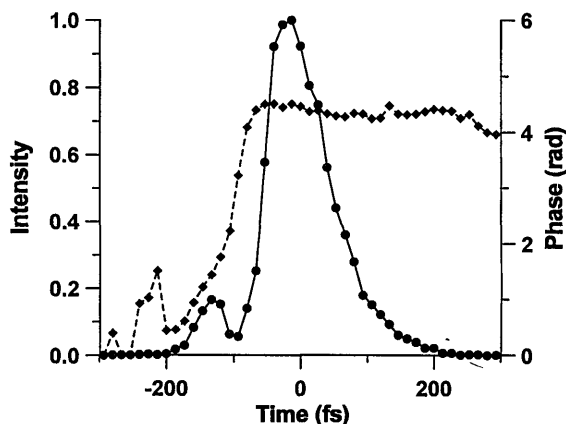
Fig. 9. Electric-field intensity (solid curve with circles) and phase (dashed curve with diamonds) associated with the SHG FROG trace of Fig. 7. The π-phase-shifted satellite pulse is indicative of spectral cubic phase distortion. The convergence parameter was $G = 0.00350$.
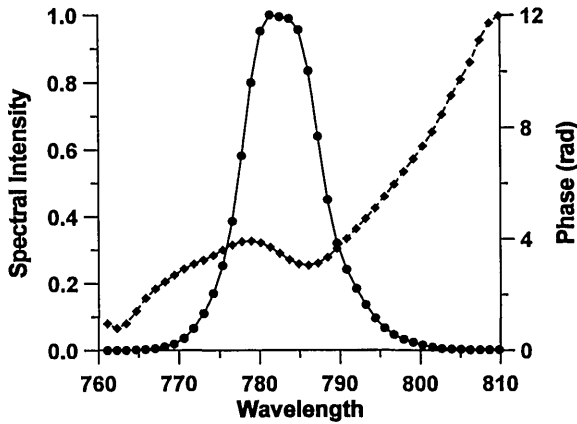
Fig. 10. Spectral intensity (solid curve with circles) and phase (dashed curve with diamonds) of the pulse of Fig. 8. Here we see clearly the cubic dependence of the phase in the spectral domain.
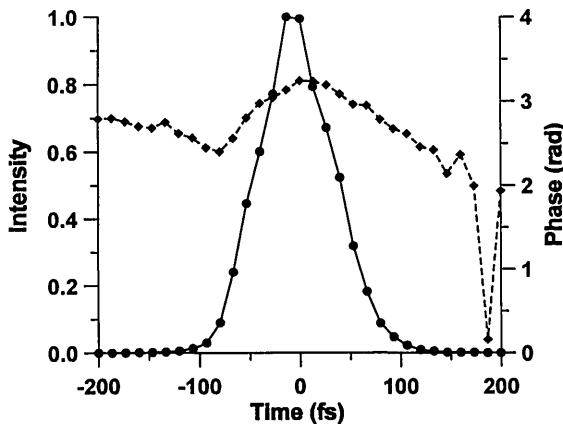
Fig. 11. Intensity (solid curve with circles) and phase (dashed curve with diamonds) pulse from a Ti:sapphire laser retrieved through SHG FROG ($G = 0.00312$) before propagation through BK7 glass. The pulse, centered near 750 nm, is 90 fs wide (FWHM).

oscillator operating near 780 nm when a large amount of glass was present in the cavity. The experimental data were taken at 43 separate time delays. We see the horseshoe characteristic that is indicative of spectral cubic phase distortion.[14] The retrieved electric field in the time domain is shown in Fig. 9, where G was 0.00350 on a 128 × 128-pixel FROG trace. This pulse shows the phase-shifted satellite pulse characteristic of spectral cubic phase distortion. The intensity and the phase of the spectrum, shown in Fig. 10, confirm this observation. Here the cubic component of the spectral phase is clearly visible. Thus we see that it is indeed possible to retrieve temporally nonsymmetric pulses, as well as those with higher-order phase distortions, by means of SHG FROG.

Finally, we have also tested the accuracy of the SHG FROG algorithm by imparting a known phase distortion to a pulse. We took the pulse shown in Fig. 11 (measured by SHG FROG, where $G = 0.00312$), which is a nearly transform-limited pulse at a wavelength of 750 nm with a FWHM of 90 fs, and propagated it through 6.5 cm of BK7 glass. We then measured the resulting lengthened pulse with SHG FROG, with the resulting electric field shown in Fig. 12 ($G = 0.00270$). We see that the pulse has spread

to a FWHM of 179 fs and has acquired a strong quadratic phase, with $b = 8.3 \times 10^{-5}$ fs^{-2}. By numerically propagating the pulse of Fig. 11 through 6.5 cm of BK7 glass [group-velocity dispersion of 495 fs^2/cm (Ref. (24)], we obtain a pulse with a FWHM of 169 fs and a chirp parameter of $b = 8.0 \times 10^{-5}$ fs^{-2}, both of which are within 6% of the measured values. This measurement confirms that it is indeed possible to measure the phase of a pulse quite accurately by using SHG FROG.

Finally, one advantage of SHG FROG that has not been noted previously is the potential for high-dynamic-range measurements. This potential occurs because in SHG FROG the signal field is at a different frequency than that of the input fields, and thus SHG FROG is totally immune to scattering of the input fields. The main source of optical noise is scattering of the second harmonic of the input fields, which is much smaller in intensity. We can therefore expect high-dynamic-range measurements to be possible. This is illustrated in Fig. 13. Here we have plotted the retrieved ($G = 0.00108$) intensity in the time and frequency domains on a logarithmic scale. We see that the noise floor of the retrieved pulse is roughly 10^{-4}. The data had a maximum of 30,226 counts, with 1–3 counts of residual dark-current noise after background subtraction. We therefore see that the dynamic range of the retrieved pulse is essentially limited by the dynamic range of the input data. With care, the dynamic range of the data in a SHG FROG experiment can be increased even further.

7. SUMMARY

We have discussed both the experimental and the algorithmic implementation of SHG FROG. We have presented a new, much more robust algorithm for retrieving the complete intensity and phase of pulses measured with this technique. We discussed experimental limitations and showed experimental confirmation of the accuracy of the technique. We have demonstrated the technique on several pulses, including one with cubic spectral phase distortion.
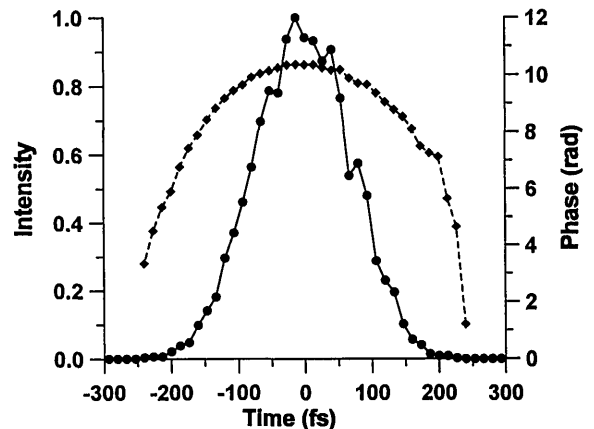
Fig. 12. Intensity (solid curve with circles) and phase (dashed curve with diamonds) of the pulse of Fig. 11 after propagation through 6.5 cm of BK7 glass. The pulse has broadened to 179 fs and has acquired a substantial quadratic phase. The width and the phase curvature of this pulse ($G = 0.00270$) are extremely close to predictions from theory (see the text).
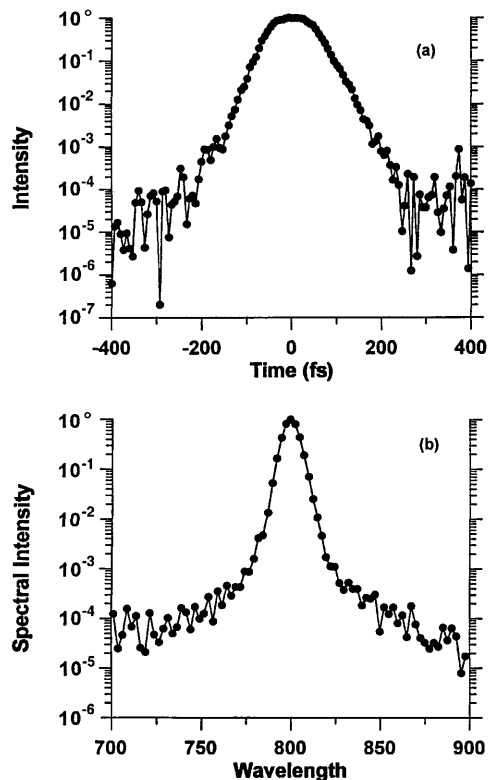
Fig. 13. SHG FROG can achieve a large dynamic range in the retrieved pulse. Here we see the (a) temporal and the (b) spectral intensities of a pulse retrieved with SHG FROG ($G = 0.00108$) plotted on a logarithmic scale. The dynamic range of the retrieved pulse is limited by the dynamic range of the data, which had a maximum of 30,226 photoelectron counts and a noise background of 1–3 counts.

Although SHG FROG faces some difficulties compared with FROG that uses third-order nonlinearities (an ambiguity in the direction of time, traces that do not contain much intuitive information, and a somewhat less robust algorithm), we think it will become a valuable tool for pulses that are too weak to be measured with third-order techniques. Also, SHG FROG is useful when high-dynamic-range measurements are needed.

ACKNOWLEDGMENTS

Note added in proof: It has come to our attention that the first experimental SHG FROG traces were reported by Ishida *et al.*[25] rather than in Ref. 16, although the intensity and the phase of the pulse were not recovered.

REFERENCES

1. E. P. Ippen and C. V. Shank, "Techniques for measurement," in *Ultrashort Light Pulses—Picosecond Techniques and Applications*, S. L. Shapiro, ed. (Springer-Verlag, Berlin, 1977), p. 83.
2. J. A. Giordmaine, P. M. Rentzepis, S. L. Shapiro, and K. W. Wecht, "Two-photon excitation of fluorescence by picosecond light pulses," Appl. Phys. Lett. **11**, 216–218 (1967).
3. S. M. Saltiel, K. A. Stankov, P. D. Yankov, and L. I. Telegin, "Realization of a diffraction-grating autocorrelator for single-shot measurement of ultrashort light pulse duration," Appl. Phys. B **40**, 25–27 (1986).
4. J.-C. M. Diels, J. J. Fontaine, I. C. McMichael, and F. Simoni, "Control and measurement of ultrashort pulse shapes (in amplitude and phase) with femtosecond accuracy," Appl. Opt. **24**, 1270–1282 (1985).
5. K. Naganuma, K. Mogi, and H. Yamada, "General method for ultrashort pulse chirp measurement," IEEE J. Quantum Electron. **25**, 1225–1233 (1989).
6. J. L. A. Chilla and O. E. Martinez, "Direct determination of the amplitude and the phase of femtosecond light pulses," Opt. Lett. **16**, 39–41 (1991).
7. M. Beck, M. G. Raymer, I. A. Walmsley, and V. Wong, "Chronocyclic tomography for measuring the amplitude and phase structure of optical pulses," Opt. Lett. **18**, 2041–2043 (1993).
8. V. Wong and I. A. Walmsley, "Analysis of ultrashort pulse-shape measurements using linear interferometers," Opt. Lett. **19**, 287–289 (1994).
9. V. Wong and I. Walmsley, "Pulse-shape measurement using linear interferometers," in *Generation, Amplification Measurement of Ultrashort Laser Pulses*, R. P. Trebino and I. A. Walmsley, eds., Proc. Soc. Photo-Opt. Instrum. Eng. **2116**, 254–267 (1994).
10. D. J. Kane and R. Trebino, "Single-shot measurement of the intensity and phase of an arbitrary ultrashort pulse by using frequency-resolved optical gating," Opt. Lett. **18**, 823–825 (1993).
11. D. J. Kane and R. Trebino, "Characterization of arbitrary femtosecond pulses using frequency-resolved optical gating," IEEE J. Quantum Electron. **29**, 571–579 (1993).
12. R. Trebino and D. J. Kane, "Using phase retrieval to measure the intensity and phase of ultrashort pulses: frequency-resolved optical gating," J. Opt. Soc. Am. A **10**, 1101–1111 (1993).
13. D. J. Kane, A. J. Taylor, R. Trebino, and K. W. DeLong, "Single-shot measurement of the intensity and phase of a femtosecond UV laser pulse with frequency-resolved optical gating," Opt. Lett. **19**, 1061–1063, (1994).
14. K. W. DeLong, R. Trebino, and D. J. Kane, "Comparison of ultrashort-pulse frequency-resolved-optical-gating traces for three common beam geometries," J. Opt. Soc. Am. B **11**, 1595–1608 (1994).
15. D. J. Kane and R. Trebino, U.S. patent application 07/966,644 (October 26, 1992).
16. J. Paye, M. Ramaswamy, J. G. Fujimoto, and E. P. Ippen, "Measurement of the amplitude and phase of ultrashort light pulses from spectrally resolved autocorrelation," Opt. Lett. **18**, 1946–1948 (1993).
17. K. W. DeLong and R. Trebino, "Improved ultrashort pulse-retrieval algorithm for frequency-resolved optical gating," J. Opt. Soc. Am. A **11**, 2429–2437 (1994).
18. A. E. Siegman, *Lasers* (University Science, Mill Valley, Calif., 1986), Chap. 9.
19. J. R. Fienup, "Phase retrieval algorithms: a comparison," Appl. Opt. **21**, 2758–2769 (1982).
20. A. Levi and H. Stark, "Restoration from phase and magnitude by generalized projections," in *Image Recovery: Theory and Applications*, H. Stark, ed. (Academic, San Diego, Calif., 1987), pp. 277–320.
21. W. H. Press, W. T. Vetterling, and S. A. Teukolsky, *Numerical Recipes in C: Second Edition* (Cambridge U. Press, Cambridge, 1992), pp. 420–425.
22. F. A. Hopf and G. I. Stegeman, *Applied Classical Electrodynamics* (Wiley, New York, 1986), Vol. II.
23. A. M. Weiner, "Effect of group velocity mismatch on the measurement of ultrashort optical pulses via second harmonic generation," IEEE J. Quantum Electron. **19**, 1276–1283 (1983).
24. *Schott Computer Glass Catalog 1.0* (Schott Glasswerke, Mainz, Germany, 1992).
25. Y. Ishida, K. Naganuma, and T. Yajima, IEEE J. Quantum Electron. **QE-21**, 69–77 (1985).